Waveform inversion for microseismic source parameters: Synthetic and field-data applications

Oscar Jarillo Michel and Ilya Tsvankin
Center for Wave Phenomena, Colorado School of Mines

ABSTRACT

Accurate estimation of the source parameters is a major task in microseimic monitoring. Here, we employ elastic waveform inversion (WI) to estimate the location, origin time, and seismic moment tensor of microseismic sources embedded in 2D VTI (transversely isotropic with a vertical symmetry axis) media. Forward modeling is carried out with a finite difference code that generates P- and SV-waves from dislocation-type sources. In addition to minimization of the objective function with a constant step length, we apply the nonlinear conjugate gradient method (NCG) for model updating. The WI algortihm is shown to be stable in the presence of moderate random Gaussian noise. We also present preliminary results of testing the WI methodology on a data set from Bakken field, North Dakota. Matching the P- and SV-waveforms from a microseismic event recorded in a near-vertical well provides an improved source location along with estimates of the pertinent components of the moment tensor.

1 INTRODUCTION

Microseismic monitoring is a rapidly developing technology essential for understanding the behavior of hydraulic fractures in unconventional plays. Microseismic methods are designed to find the spatial and temporal distribution of hypocenters of events triggered during hydraulic stimulation. It is also important to evaluate the mechanisms of microseismic sources by estimating their moment tensor. Conventional event-location techniques are based on picking the arrival times of the direct P- and S-waves in a borehole or at the surface (Rutledge and Scott, 2003). Also, microseismic events can be located without time picking, by employing stacking (Anikiev et al., 2014) and migration-based methods (Zhang and Zhang, 2013; Zhebel and Eisner, 2015).

Event locations are usually determined by assuming the velocity model to be known, for example from perforation shots and borehole data. However, this assumption may produce inaccurate locations if there are errors in the velocity parameters, particularly those caused by seismic anisotropy. Grechka et al. (2011) demonstrate that it is possible to construct anisotropic velocity models from traveltimes while locating microseismic events. Their method yields more accurate source locations than those based on conventional isotropic models. Furthermore, Grechka and Yaskevich (2013, 2014) demonstrate that microseismic surveys with sufficient angle coverage provide enough information to build layered triclinic (i.e., most general anisotropic) models.

Most existing algorithms invert for the seismic moment tensor $\mathbf{M}$ under the assumption that the source position $\mathbf{x}^s$ and origin time t_0 are known. However, migration-based and waveform inversion (WI) methods have the advantage of resolving the tensor $\mathbf{M}$ and location $\mathbf{x}^s$ simultaneously. An important difference is that migration-based techniques (Gajewski and Tessmer, 2005; Artman et al., 2010) operate in the image domain and rely on finding the maximum-energy focus point, while WI methods are based on iteratively minimizing the objective function in the data domain.

Waveform inversion is a nonlinear optimization technique that uses full-wavefield propagation for simulating the data and iteratively matches seismic waveforms to estimate the model parameters. The most attractive feature of WI is in the improved resolution of the inverted models due to the inclusion of phase and amplitude information. The advantages of WI can be exploited in microseismic studies by inverting multicomponent data for the source parameters and, potentially, for the velocity model. Jarillo Michel and Tsvankin (2014a) implement gradient calculation for the position $\mathbf{x}^s$, origin time t_0, and tensor $\mathbf{M}$ of microseismic sources embedded in VTI media using the adjoint-state method (Kim et al., 2011). That gradient-computation technique is employed by Jarillo Michel and Tsvankin (2014b) to simultaneously locate microseismic events and estimate their moment tensors. Jarillo Michel and Tsvankin (2014b) verify the accuracy of their method on synthetic data from layered VTI media.

Here, we first describe and refine the WI algorithm for estimating the source parameters presented by Jarillo Michel and Tsvankin (2014b). We introduce a line-search algorithm for model updating and discuss its benefits and shortcomings. Then, the stability of the algorithm is evaluated by adding random Gaussian noise in the frequency band of the data. Next, we apply the algorithm to a microseismic data set recorded in a vertical well at Bakken field (North Dakota, USA). Although

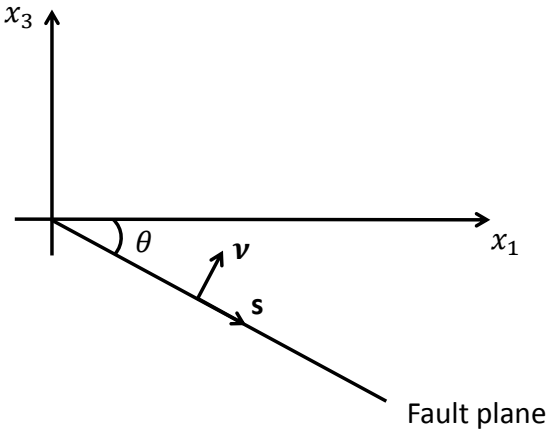

Figure 1. 2D fault geometry used in forward modeling. The vector ν is the unit fault normal, and **s** is a unit vector in the slip direction. The dip angle θ ($0^\circ \le \theta \le 90^\circ$) is measured down from the horizontal axis. The incidence plane $[x_1, x_3]$ is assumed to coincide with the dip plane of the fault and contain the slip **s**.

in general the WI methodology could operate with the entire coda, the accuracy of the velocity field is sufficient for matching the waveforms of only the direct P- and SV-arrivals.

2 OVERVIEW OF THE INVERSE PROBLEM

2.1 Forward modeling

The wave equation for a dislocation-type source located at point $\mathbf{x}^s$ in a heterogeneous anisotropic medium can be represented as (Aki and Richards, 2002):

$$\rho \frac{\partial^2 u_i}{\partial t^2} - \frac{\partial}{\partial x_j}\left(c_{ijkl}\frac{\partial u_k}{\partial x_l}\right) = -M_{ij}\frac{\partial[\delta(\mathbf{x}-\mathbf{x}^s)]}{\partial x_j} S(t)\,, \quad (1)$$

where $\mathbf{u}(\mathbf{x},t)$ is the displacement field, t is time, c_{ijkl} is the stiffness tensor ($i,j,k,l = 1,2,3$), $\rho(\mathbf{x})$ is the density, $\mathbf{M}$ is the seismic moment tensor, $S(t)$ is the source time function, and $\delta(\mathbf{x}-\mathbf{x}^s)$ is the spatial δ-function; summation over repeated indices is implied. We use finite-difference (FD) algorithm `sfewe` in MADAGASCAR to obtain the exact wavefield for VTI media from equation 1.

The VTI model considered here is described by the Thomsen (1986) parameters — the P- and S-wave vertical velocities V_{P0} and V_{S0} and the anisotropy coefficients ε and δ. Note that P- and SV-waves propagating in the $[x_1, x_3]$-plane are not influenced by the Thomsen parameter γ. The kinematic signatures of SV-waves are mostly governed by the coefficient $\sigma \equiv (V_{P0}/V_{S0})^2(\varepsilon - \delta)$ (Tsvankin, 2012).

P- and SV-waves excited by a dislocation-type source depend on the components M_{11}, M_{13}, and M_{33} of the moment tensor (Vavryčuk, 2005; Jarillo Michel and Tsvankin, 2014a) (Figure 1):

$$M_{11} = -\frac{\Sigma\bar{u}}{2}(c_{13}-c_{11})\sin 2\theta\,, \quad (2)$$

$$M_{13} = \Sigma\bar{u}c_{55}\cos 2\theta\,, \quad (3)$$

$$M_{33} = -\frac{\Sigma\bar{u}}{2}(c_{33}-c_{13})\sin 2\theta\,, \quad (4)$$

where θ is the dip of the fault, Σ is the fault area, $\bar{u}$ is the magnitude of the slip (displacement discontinuity), and c_{11}, c_{13}, c_{33}, and c_{55} are the stiffness coefficients in the two-index Voigt notation.

2.2 Inversion algorithm

Our objective is to invert for the source coordinates x_1^s and x_3^s, the origin time t_0, and the three relevant moment-tensor elements assuming that the velocity model is known. Hence, the vector of unknown model parameters is defined as:

$$\mathbf{m} = \{x_1^s, x_3^s, t_0, M_{11}, M_{13}, M_{33}\}\,. \quad (5)$$

The data residuals are measured by the least-squares objective function $\mathcal{F}$, which is minimized by the inversion algorithm:

$$\mathcal{F}(\mathbf{m}) = \frac{1}{2}\|\mathbf{d}_{\rm pre}(\mathbf{m}) - \mathbf{d}_{\rm obs}\|^2\,, \quad (6)$$

where $\mathbf{d}_{\rm pre}(\mathbf{m})$ and $\mathbf{d}_{\rm obs}$ are the predicted and observed displacements, respectively. The elastic displacement field $\mathbf{u}(\mathbf{x}^s, \mathbf{x}^{r_n}, t)$ in our simulations is excited by a single source at $\mathbf{x}^s$ and recorded by N receivers located at $\mathbf{x}^{r_n}$ ($n = 1,2,...,N$).

We use the adjoint-state method to efficiently calculate the gradient of the objective function with respect to the model parameters (Kim et al., 2011; Jarillo Michel and Tsvankin, 2014a). Although the parameters have different units, local minimization of $\mathcal{F}(\mathbf{m})$ is performed for all unknowns simultaneously. To carry out simultaneous inversion for $\mathbf{x}^s$, t_0, and $\mathbf{M}$, we employ the nondimensionalization approach suggested by Kim et al. (2011) and adapted for the problem at hand by Jarillo Michel and Tsvankin (2014a). This approach eliminates the difference between the units of different parameters and makes the gradient dimensionless. Therefore, all parameters can be updated simultaneously using a certain step length α:

$$\hat{\mathbf{m}}^{k+1} = \hat{\mathbf{m}}^k + \alpha\hat{\mathbf{g}}^k\,. \quad (7)$$

2.3 Line search for model updating

The inverse problem is nonlinear, and we solve it using an iterative local gradient-descent scheme. Because the true model in our synthetic tests is known, it is easy to select an appropriate step length to achieve fast convergence. However, implementation of this approach in practice can be problematic. It is usu-

ally more robust to compute the step length with line-search algorithms. Here, we use the line-search equation described in Gauthier et al. (1986), Virieux and Operto (2009), and Pratt (2013):

$$\alpha = \frac{(\nabla \mathcal{F})^T \mathbf{S}}{(\mathbf{JS})^T (\mathbf{JS})} , \tag{8}$$

where α is the step length, $\mathbf{S}$ is the vector of the search direction, $\mathbf{J}$ is the Fréchet matrix, and T stands for transpose. The product $\mathbf{JS}$ in the denominator of equation 8 can be approximated by perturbing the forward displacement field $\mathbf{u}(\mathbf{m})$ using a trial step length β:

$$\mathbf{JS} = \frac{\mathbf{u}(\mathbf{m}+\beta\mathbf{S}) - \mathbf{u}(\mathbf{m})}{\beta} . \tag{9}$$

Estimation of α is followed by minimization of the objective function using the nonlinear conjugate gradient (NCG) method (Nocedal and Wright, 1999), which produces fast convergence. The NCG method used here involves the following steps (k is the iteration number):

(i) Computation of the gradient direction using the adjoint-state method: $\mathbf{g}^k = \partial \mathcal{F}^k / \partial \mathbf{m}^k$.
(ii) Computation of the nondimensionalized model-parameter vector and scaled-gradient direction.
(iii) Computation of β^k using the Fletcher-Reeves formula: $\beta^k = (\hat{\mathbf{g}}^k)^T \hat{\mathbf{g}}^k / [(\hat{\mathbf{g}}^{k-1})^T \hat{\mathbf{g}}^{k-1}]$.
(iv) Updating of the conjugate direction: $\mathbf{s}^k = \hat{\mathbf{g}}^k + \beta^k \mathbf{s}^{k-1}$ (if $k = 1$, $\mathbf{s}^{k-1} = \mathbf{s}^0 = \hat{\mathbf{g}}^k$).
(v) Computation of α^k (equation 8).
(vi) Updating of the nondimensionalized model vector (equation 7).

The estimated conjugate direction loses accuracy with iterations and has to be reset to the gradient direction at least after every N iterations (N is the number of model parameters). The step length calculated by equation 8 followed by model updating using the NCG method in general provides faster convergence than a constant step length. This is due to a preconditioning operation which corrects the gradient at each iteration. For the synthetic tests below, however, the rate of convergence is similar to that achieved with a constant step length α.

Assuming that $\hat{\mathbf{m}}^k$ is located within the basin that contains the global minimum of $\mathcal{F}$, the step length should be sufficiently small to ensure that $\hat{\mathbf{m}}^{k+1}$ stays within this basin. After the update, the parameters have to be "dimensionalized" again so that they can be used as inputs for the forward modeling in the next iteration.

3 SYNTHETIC EXAMPLES

3.1 Test with line search

The tests presented by Jarillo Michel and Tsvankin (2014b) were performed using a constant step length because, as mentioned above, α could be chosen in an optimal way for a known model. In the following synthetic example we apply the line-search algorithm described above to compute the step length using the simulated wavefield.

The parameters x_1^s, x_3^s, M_{11}, M_{13}, and M_{33} are estimated for the model in Figure 2; the origin time t_0 is fixed at the actual value. The objective function (Figure 3) decreases rapidly during the initial iterations. However, the convergence slows

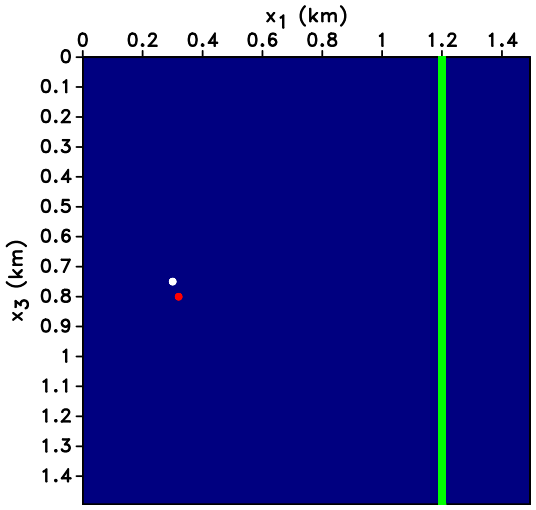

Figure 2. Actual source (white dot), trial source (red dot) and a vertical line of receivers (spacing is 6 m) embedded in a homogeneous VTI medium. The medium parameters are $\rho = 2$ g/cm^3, $V_{P0} = 4047$ m/s, $V_{S0} = 2638$ m/s, $\varepsilon = 0.4$, and $\delta = 0$. The actual source is located at $x_1 = 0.3$ km and $x_3 = 0.75$ km with $\theta = 0^\circ$ (see equations 2 – 4). For the trial source, $x_1 = 0.32$ km, $x_3 = 0.8$ km, and $\theta = 15^\circ$. Both events occur at the same time ($t_0 = 0.049$ s) and have the same $\Sigma \bar{u} = 1$ m^3.

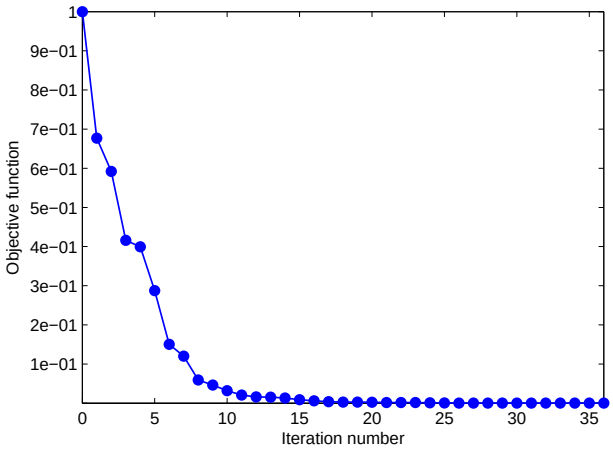

Figure 3. Change of the normalized objective function $\mathcal{F}(\mathbf{m})$ with iterations for the model in Figure 2. Parameter updating was carried out with the NCG method. The origin time t_0 is fixed at the correct value.

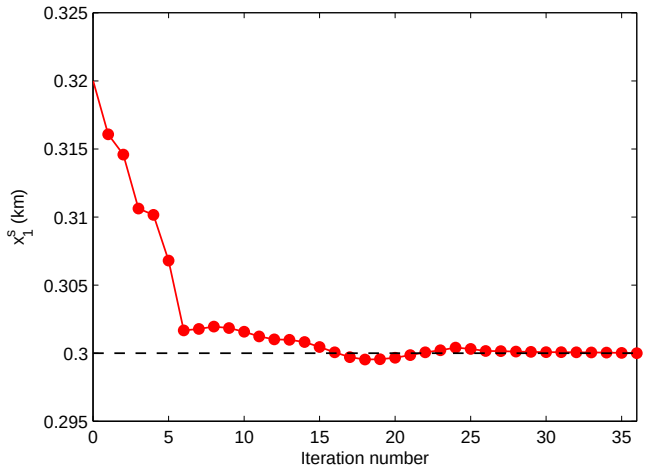

(a)

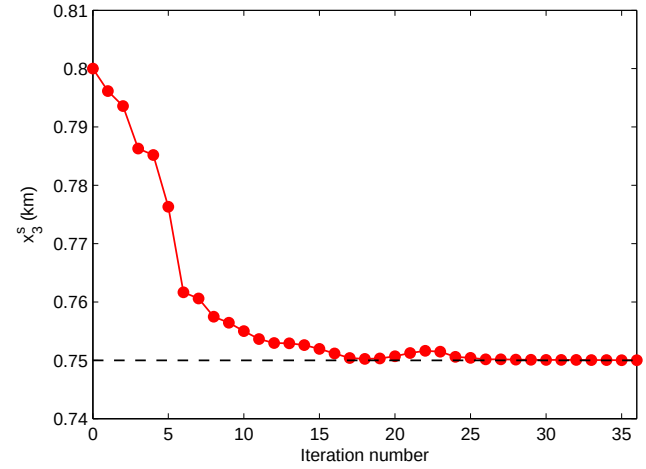

(b)

Figure 4. Change of the source coordinates (a) x_1^s and (b) x_3^s with iterations for the model in Figure 2. The actual values are marked by dashed lines.

down after the ninth iteration, when the estimated source position is only about 5 m away from the actual location. In that case, equation 8, which depends on the difference $[\mathbf{u}(\mathbf{m}+\beta\mathbf{S})-\mathbf{u}(\mathbf{m})]/\beta$, minimizes the objective function more slowly because the location error is smaller than the grid spacing (which in this example is 6 m). Still, the model obtained after six iterations is within the limits of seismic resolution (Figures 4 and 5). To overcome this issue, the grid size has to be defined according to the required precision in the source location.

Employing a constant step length allows the updating algorithm to avoid this problem because there is no step-length calculation involved (Figure 6), and the update is independent of grid spacing. However, choosing an optimal step length in field-data applications may be challenging.

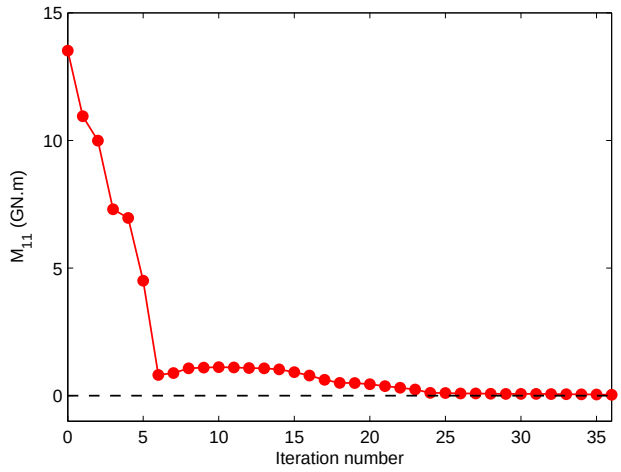

(a)

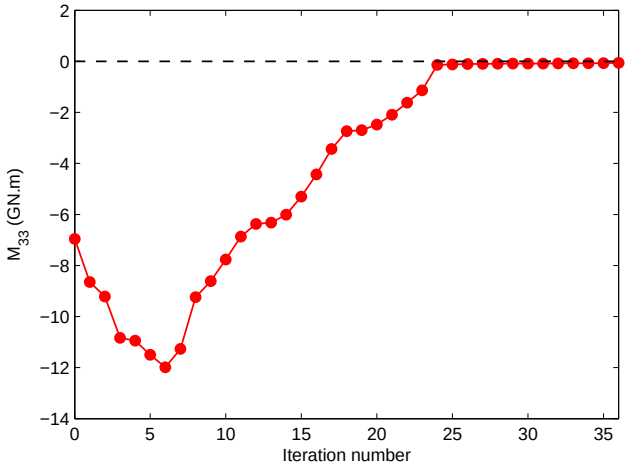

(b)

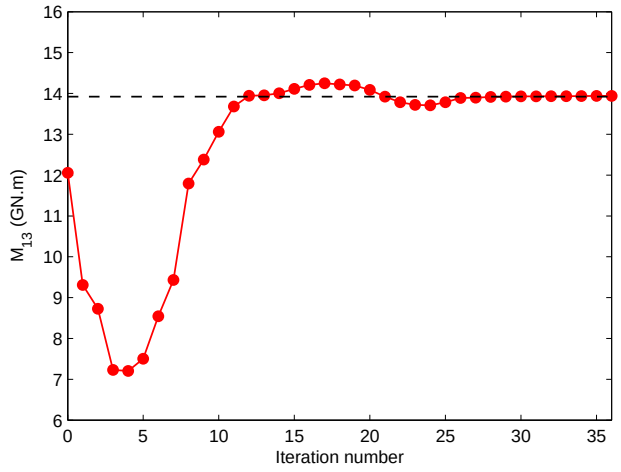

(c)

Figure 5. Change of the moment-tensor elements (a) M_{11}, (b) M_{33}, and (c) M_{13} with iterations for the model in Figure 2.

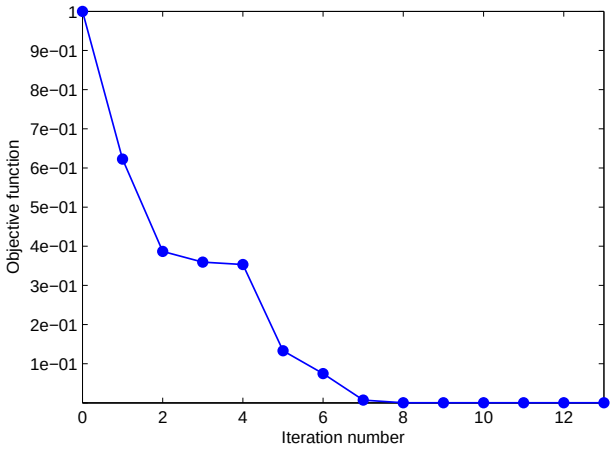

Figure 6. Change of the normalized objective function $\mathcal{F}(\mathbf{m})$ with iterations for the model in Figure 2. Parameter updating was carried out with a constant step length. The origin time t_0 is fixed at the correct value.

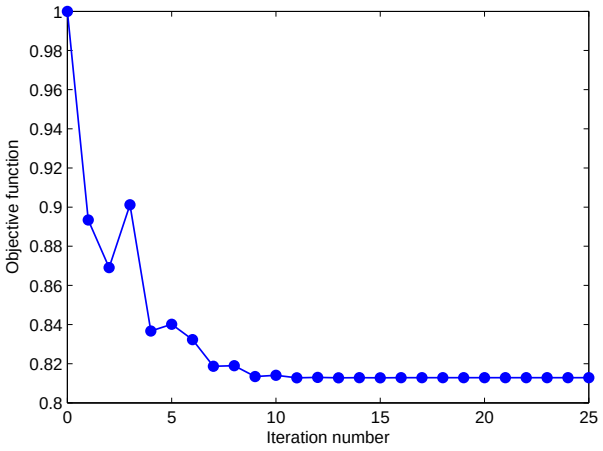

Figure 8. Change of the normalized objective function $\mathcal{F}(\mathbf{m})$ with iterations for the model in Figure 2. The inversion was performed on noise-contaminated data (see Figure 7).

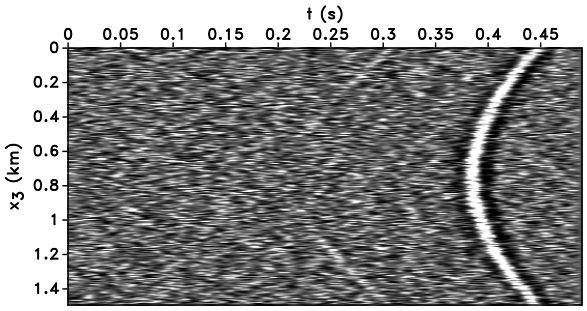

Figure 7. Vertical displacement of the observed data contaminated with Gaussian noise for the model in Figure 2. The noise has the same frequency band as the data and the variance is equal to 0.07% of the maximum amplitude.

3.2 Test with noise

It is important to evaluate the influence of noise in the input data on the inversion results. We use the homogeneous VTI model from Figure 2 and add random Gaussian noise in the frequency band of the observed data with the variance equal to 0.07% of the maximum amplitude. The noise does not completely mask the arrivals but creates significant distortions in the seismogram (Figure 7). The inversion algorithm, applied with a constant step length, estimates $\mathbf{x}^s$ and $\mathbf{M}$, whereas the origin time t_0 is fixed at the actual value. The objective function (Figure 8) is not monotonic and, as expected, flattens out at a larger value than that in the noise-free test (Figure 6).

Still, despite the substantial magnitude of noise, the errors in the estimated source coordinates (Figure 9) and the moment-tensor elements M_{11} and M_{33} (Figure 10) are relatively small. The inverted parameter M_{13}, which is most sensitive to waveform matching, deviates by about 16% from the actual value. Because the noise influences mainly the amplitudes, one would expect it to distort the tensor $\mathbf{M}$ more than the coordinates $\mathbf{x}^s$, which is indeed the case. However, as discussed above, the gradient for the source coordinates depends on $\mathbf{M}$, which causes small errors in x_1^s and x_3^s (Figure 9). For this model, the variance of Gaussian noise has to reach about 20% of the maximum amplitude for the line search to get trapped in local minima.

4 MICROSEISMIC DATA SET

The microseismic survey made available to us by Marathon Oil Company was recorded to test engineering parameters for hydraulic stimulations at Bakken field. The complete data set contains over 900 located microseismic events triggered during a hydraulic stimulation of a well. The section at Bakken field is mainly composed of five formations: the Lodgepole limestone (LP), Upper Bakken shales (UB), Middle Bakken sandstones and siltstones (MB), Lower Bakken shales (LB), and the Three Forks (TF) dolomites (Table 1):

Conventional processing of the microseismic events was carried out by a service company that acquired the data. The events were originally located using a horizontally-layered isotropic velocity model obtained from sonic logs, perforation shots, and sleeve-opening data. Grechka and Yaskevich (2014) demonstrate that the isotropic model is insufficient for accurate event location because cores collected in the Lower Bakken shale exhibit strong anisotropy. Using traveltime picks of the direct P-, S_1-, and S_2-waves recorded by geophones in two monitor wells, they invert for the velocity parameters, hypocenter coordinates, and event origin times. They prove that waves excited by microseismic sources provide sufficient subsurface illumination for constraining layer-based

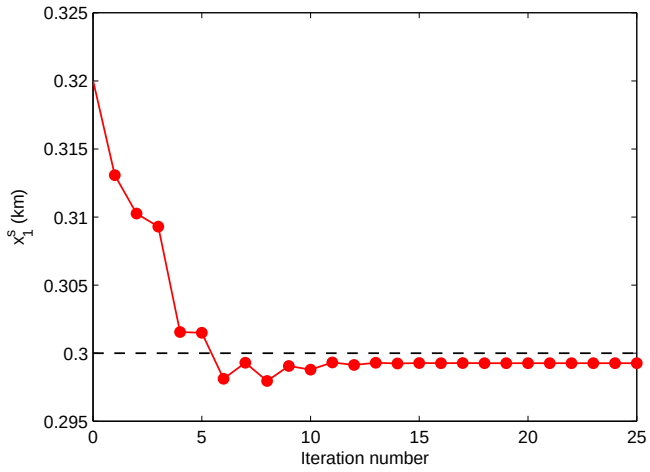

(a)

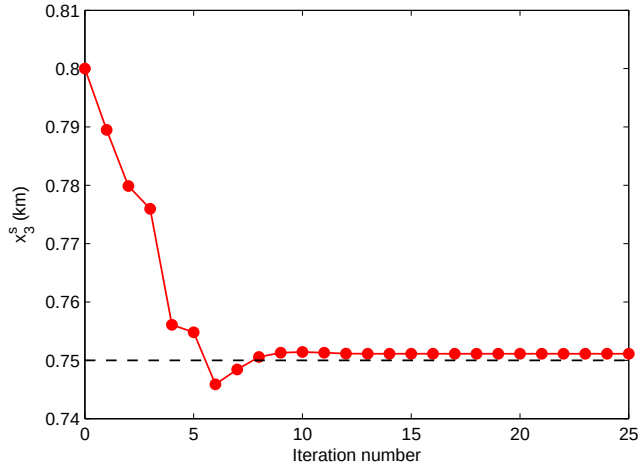

(b)

Figure 9. Change of the source coordinates (a) x_1^s and (b) x_3^s with iterations for the model in Figure 2. The inversion was performed on noise-contaminated data (see Figure 7).

Layer	V_{P0} (m/s)	V_{S0} (m/s)	ε	δ	γ	ρ (g/cm^3)
LP	4560	2720	0.10	0.07	0.02	2660
UB	3160	2010	0.37	-0.01	0.33	2660
MB	4630	2830	0.01	0.17	-0.12	2640
LB	2810	1970	0.27	0.19	0.35	2610
TF	4170	2380	0.09	0.16	0.13	2300

Table 1. Parameters of five layers (LP, UB, MB, LB, and TF) at Bakken field obtained by Grechka and Yaskevich (2014). The top three layers (LP, UB, MB) were found to be triclinic but the table lists the closest VTI model for each.

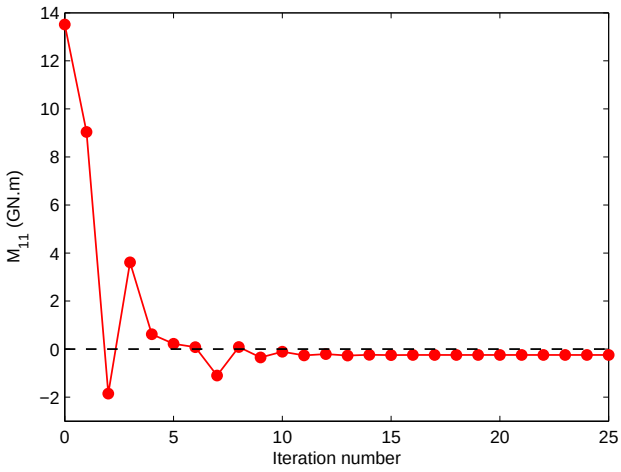

(a)

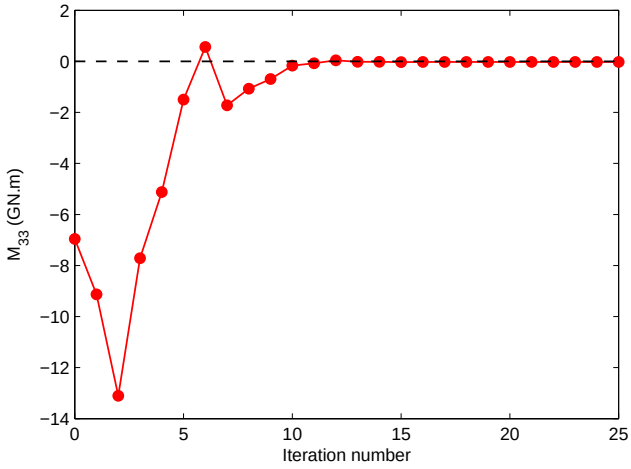

(b)

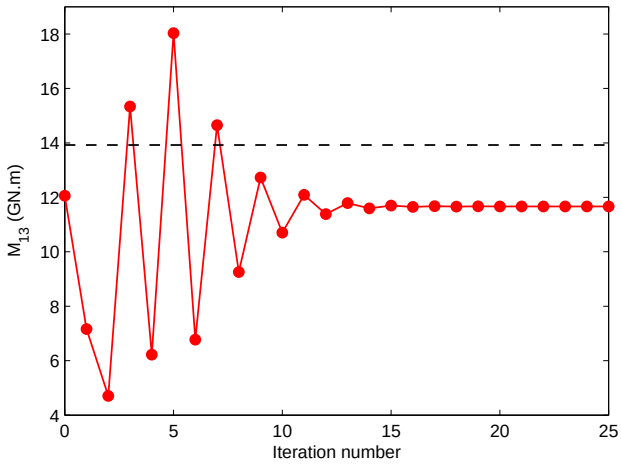

(c)

Figure 10. Change of the moment-tensor elements (a) M_{11}, (b) M_{33}, and (c) M_{13} with iterations for the model in Figure 2. The inversion was performed on noise-contaminated data (see Figure 7).

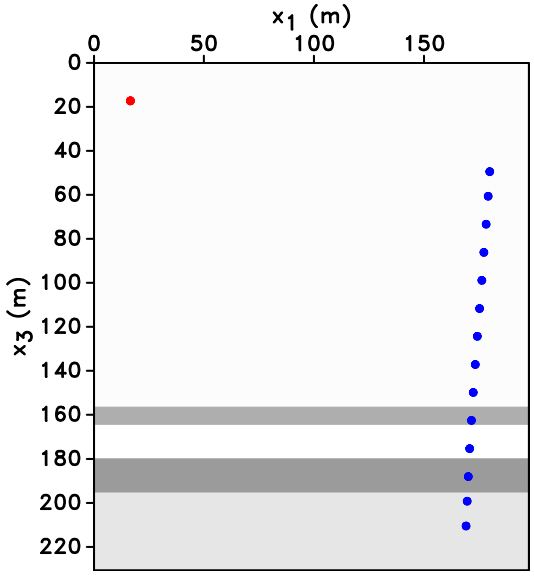

Figure 11. Acquisition geometry for the microseismic survey at Bakken field. Microseismic event (red dot) and a tilted array of receivers (blue dots) are embedded in a layered VTI medium. The average spacing between the receivers is 12.39 m. The medium parameters are listed in Table 1. The initial source location is $x_1 = 16.52$ m, $x_3 = 17.29$ m.

anisotropy parameters. Grechka and Yaskevich (2014) build a layered anisotropic model that includes triclinic and VTI horizons and show that taking anisotropy into account provides more accurate locations and tightens event clouds.

5 DATA PROCESSING

The majority of microseismic events occur in the Lodgepole (LP) formation, about 150 m above the stimulated well. Here, we present preliminary processing results for one of the events triggered during the well treatment. Event registration was performed in two near-vertical monitor wells, one of which (with 14 receivers) is used here (Figure 11). The traces for the bottom three receivers have a low signal-to-noise ratio and were removed.

Grechka and Yaskevich (2014) identify pronounced shear-wave splitting, with the fast S_1-wave polarized nearly horizontally (SH) and the slow S_2-wave polarized close to the vertical incidence plane (SV). For inversion purposes, we process only the P- and SV-wave arrivals because SH-waves cannot be simulated by our modeling code. Also, the accuracy of the velocity model is insufficient for modeling the coda formed by multiples, scattered waves, etc., so we window the seismogram to focus on the direct P- and SV-waves. Including velocity analysis in the inversion algorithm could allow us to take advantage of the coda in the future.

Here, we present preliminary results of WI for the microseismic event in Figure 11. The velocity model is taken from the work of Grechka and Yaskevich (2014); the origin time and initial position of the source were provided to us by Dr. Grechka. Our goal is to refine the source position $\mathbf{x}^s$ (Figure 11) and estimate the tensor $\mathbf{M}$ of this event. Waveform fitting is limited to the windowed direct P- and SV- arrivals recorded on the vertical component and the P-arrivals recorded on the horizontal component (Figures 12 and 13).

The wavelet needed for the simulation was extracted from the relatively clean P-wave arrival on the horizontal component of the fourth receiver from the top (Figure 14). Also, P-waves are less influenced by attenuation, which makes them more suitable for wavelet estimation. No estimates of the moment-tensor elements were available to us. Therefore, the initial values of M_{11}, M_{13}, and M_{33} correspond to a horizontal double-couple source ($\theta = 0$, see equations 2 - 4) that generates the displacement amplitude close to the one in the observed data.

The initial model produces significant data residuals, mostly because of a poor approximation for the moment tensor (Figure 15). After the inversion, the data fit is substantially improved and the objective function is reduced by 66%. The updated source location after the inversion is $x_1 = 14$ m, $x_3 = 16.47$ m and the estimated moment-tensor elements are $M_{11} = 4.49\text{x}10^{10}$ GN $\cdot$ m, $M_{33} = -3.22\text{x}10^{10}$ GN $\cdot$ m, and $M_{13} = 4.8\text{x}10^{10}$ GN $\cdot$ m.

6 CONCLUSIONS

We presented a refinement of our previously published WI method for microseismic data by introducing line search for model updates. Our algorithm is designed to estimate the parameters (location, origin time and moment tensor) of microseismic sources for 2D elastic VTI media. Applying line search for step-length calculation should improve the inversion results for field data because it is difficult to choose an optimal constant step length without knowledge of the model parameters. However, line-search algorithms are subject to resolution and precision limitations related to grid spacing.

To assess the stability of the algorithm, the input data were contaminated with Gaussian noise in the frequency band of the observed data and the variance equal to 0.07% of the maximum amplitude. Although the objective function is not reduced nearly as much as in noise-free tests, the only noticeably distorted parameter is M_{13}. If the variance of the noise reaches 20% of the maximum amplitude, the inversion gets trapped in local minima.

The WI methodology is tested on a data set from Bakken field. Although the inversion can operate with the entire seismic trace, here we only use the direct P- and SV-waves due to limitations of the velocity model. The preliminary results prove the feasibility of constraining the source parameters by matching the waveforms recorded by multicomponent receivers in a single near-vertical well.

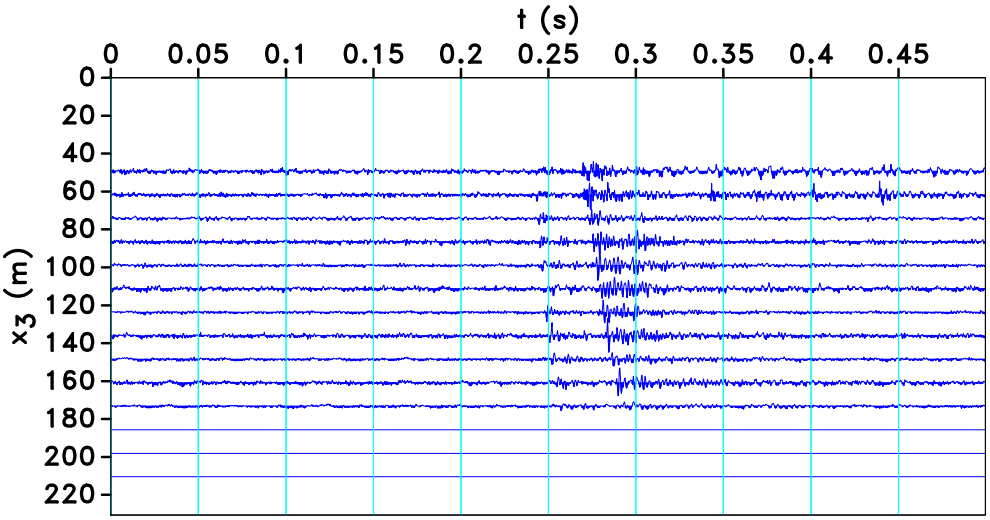

Figure 12. Vertical component of the recorded displacement after removal of the three bottom traces.

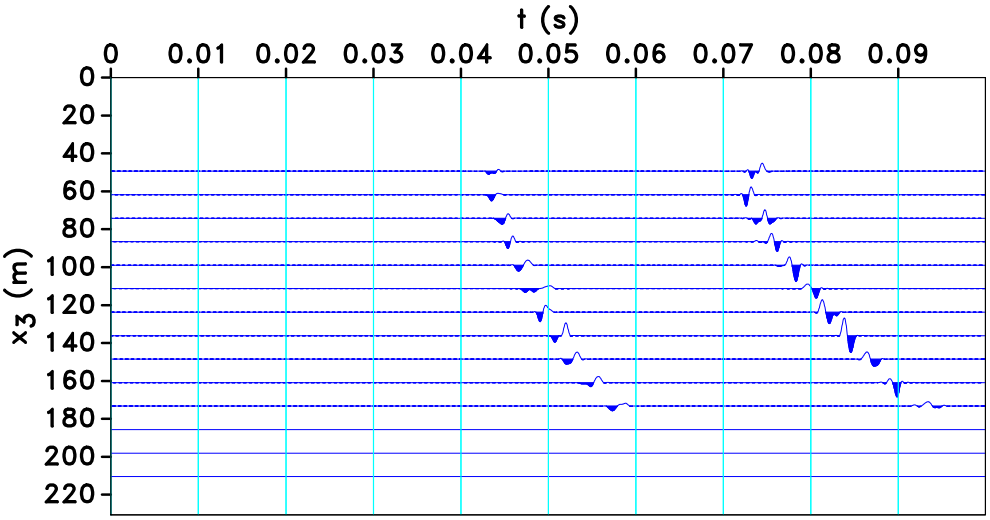

Figure 13. Vertical component of the recorded displacement after windowing of the direct P- and SV-waves.

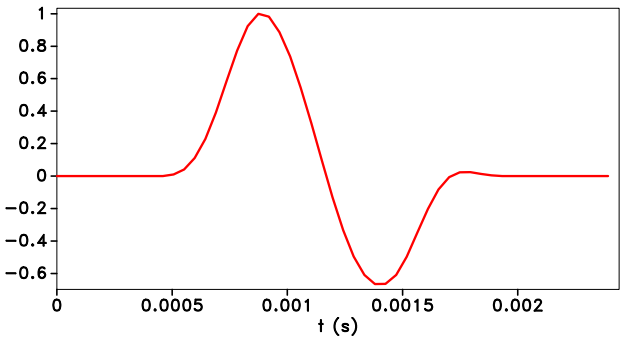

Figure 14. Wavelet extracted from the P-wave arrival on the horizontal component.

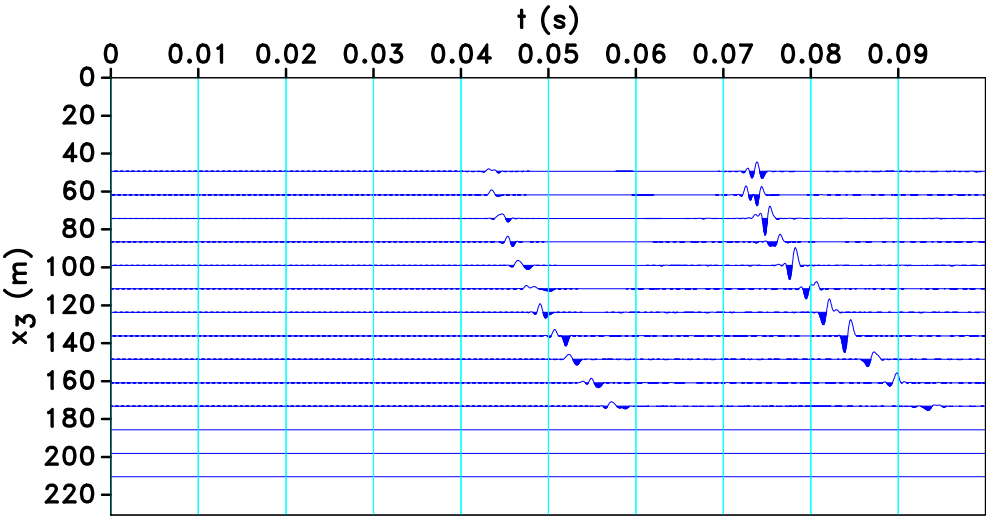

Figure 15. Difference between the recorded vertical displacement (Figure 13) and the displacement computed for the initial model. The scale is the same as in Figure 13.

7 ACKNOWLEDGMENTS

We are grateful to Vladimir Grechka (Marathon Oil), who generously provided the data set and valuable insights and feedback regarding various aspects of this work. The modeling and inversion results in this paper are produced with the MADAGASCAR open-source software package freely available at www.ahay.org. This work was supported by the Consortium Project on Seismic Inverse Methods for Complex Structures at the Center for Wave Phenomena (CWP).

REFERENCES

Aki, K., and P. G. Richards, 2002, Quantitative seismology: University Science Books.

Anikiev, D., J. Valenta, F. Staněk, and L. Eisner, 2014, Joint location and source mechanism inversion of microseismic events: benchmarking on seismicity induced by hydraulic fracturing: Geophysical Journal International, **198**, 249–258.

Artman, B., I. Podladtchikov, and B. Witten, 2010, Source location using time-reverse imaging: Geophysical Prospecting, **58**, 861–873.

Gajewski, D., and E. Tessmer, 2005, Reverse modelling for seismic event characterization: Geophysical Journal International, **163**, 276–284.

Gauthier, O., J. Virieux, and A. Tarantola, 1986, Two-dimensional nonlinear inversion of seismic waveforms: Numerical results: Geophysics, **51**, 1387–1403.

Grechka, V., P. Singh, and I. Das, 2011, Estimation of effective anisotropy simultaneously with locations of microseismic events: Geophysics, **76**, WC143–WC155.

Grechka, V., and S. Yaskevich, 2013, Inversion of microseismic data for triclinic velocity models: Geophysical Prospecting, **61**, 1159–1170.

———, 2014, Azimuthal anisotropy in microseismic monitoring: A Bakken case study: Geophysics, **79**, KS1–KS12.

Jarillo Michel, O., and I. Tsvankin, 2014a, Gradient calculation for waveform inversion of microseismic data in VTI media: Journal of Seismic Exploration, **23**, 201–217.

———, 2014b, Waveform inversion for parameters of microseismic sources in VTI media: CWP Project Review Report, 193–204.

Kim, Y., Q. Liu, and J. Tromp, 2011, Adjoint centroid-moment tensor inversions: Geophysical Journal International, **186**, 264–278.

Nocedal, J., and S. J. Wright, 1999, Numerical optimization: Springer.

Pratt, R., 2013, Waveform tomography an introduction to theory and practice: Western Science.

Rutledge, J. T., and P. W. Scott, 2003, Hydraulic stimulation of natural fractures as revealed by induced microearthquakes, Carthage Cotton Valley gas field, east Texas: Geophysics, **68**, 441–452.

Thomsen, L., 1986, Weak elastic anisotropy: Geophysics, **51**, 1954–1966.

Tsvankin, I., 2012, Seismic signatures and analysis of reflection data in anisotropic media, third edition: Society of Exploration Geophysicists.

Vavryčuk, V., 2005, Focal mechanisms in anisotropic media: Geophysical Journal International, **161**, 334–346.

Virieux, J., and S. Operto, 2009, An overview of full-waveform inversion in exploration geophysics: Geophysics, **74**, WCC1–WCC26.

Zhang, W., and J. Zhang, 2013, Microseismic migration by semblance-weighted stacking and interferometry: SEG Technical Program Expanded Abstracts, 2045–2049.

Zhebel, O., and L. Eisner, 2015, Simultaneous microseismic event localization and source mechanism determination: Geophysics, **80**, KS1–KS9.